U.S. Department of
Transportation
**Federal Railroad
Administration**

Analyses of Rail Chill Effect

Office of Research
and Development
Washington, DC 20590

Research and Special Programs Administration
John A. Volpe National Transportation Systems Center
Cambridge, MA 02142-1093

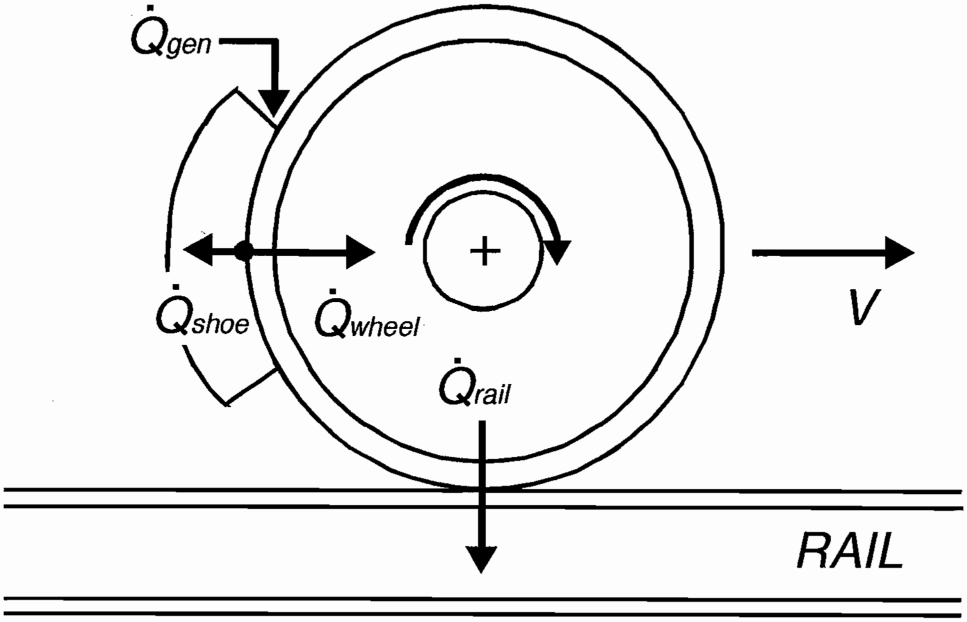

DOT/FRA/ORD-97/07
DOT-VNTSC-FRA-96-8

Final Report
June 1998

This document is available to the public through the National
Technical Information Service, Springfield, VA 22161

NOTICE

This document is disseminated under the sponsorship of the Department of Transportation in the interest of information exchange. The United States Government assumes no liability for its contents or use thereof.

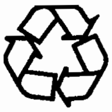

REPORT DOCUMENTATION PAGE

Form Approved
OMB No. 0704-0188

Public reporting burden for this collection of information is estimated to average 1 hour per response, including the time for reviewing instructions, searching existing data sources, gathering and maintaining the data needed, and completing and reviewing the collection of information. Send comments regarding this burden estimate or any other aspect of this collection of information, including suggestions for reducing this burden, to Washington Headquarters Services, Directorate for Information Operations and Reports, 1215 Jefferson Davis Highway, Suite 1204, Arlington, VA 22202-4302, and to the Office of Management and Budget, Paperwork Reduction Project (0704-0188), Washington, DC 20503.

1. AGENCY USE ONLY (Leave blank)	2. REPORT DATE June 1998	3. REPORT TYPE AND DATES COVERED Final Report November 1994 - March 1995

4. TITLE AND SUBTITLE
Analyses of Rail Chill Effect

5. FUNDING NUMBERS
R8005/RR828

6. AUTHOR(S)
K. E. Crowe and P. K. Raj

7. PERFORMING ORGANIZATION NAME(S) AND ADDRESS(ES)
Technology & Management Systems, Inc.*
99 South Bedford St., Suite 211
Burlington, MA 01803

8. PERFORMING ORGANIZATION REPORT NUMBER
DOT-VNTSC-FRA-96-8

9. SPONSORING/MONITORING AGENCY NAME(S) AND ADDRESS(ES)
U.S. Department of Transportation
Federal Railroad Administration
Office of Research and Development
Washington, DC 20590

10. SPONSORING/MONITORING AGENCY REPORT NUMBER
DOT/FRA/ORD-97/07

11. SUPPLEMENTARY NOTES
*under contract to: U.S. Department of Transportation
Research and Special Programs Administration
Volpe National Transportation Systems Center
Cambridge, MA 02142-1093

12a. DISTRIBUTION/AVAILABILITY STATEMENT
This document is available to the public through the National Technical Information Service, Springfield, VA 22161

12b. DISTRIBUTION CODE

13. ABSTRACT (Maximum 200 words)

The principles of heat transfer are applied to analyze the so-called "rail chill" effect, which refers to heat loss by conduction from a hot rail vehicle wheel through the contact area into a cold rail, the wheel having been heated by friction braking. A difference of more than a factor of two is demonstrated between chill effectiveness based on instantaneous heat generation and transfer rates, and the total heat lost to the rail, as a percentage of the total heat generated over a specific period of time, in transient situations such as stop braking.

14. SUBJECT TERMS
Braking; Heat transfer analysis; Rail vehicles; Wheels

15. NUMBER OF PAGES
56

16. PRICE CODE

17. SECURITY CLASSIFICATION OF REPORT Unclassified	18. SECURITY CLASSIFICATION OF THIS PAGE Unclassified	19. SECURITY CLASSIFICATION OF ABSTRACT Unclassified	20. LIMITATION OF ABSTRACT Unlimited

NSN 7540-01-280-5500

Standard Form 298 (Rev. 2-89)
Prescribed by ANSI Std. 239-18
298-102

PREFACE

This report is the eighth in a series of engineering studies on railroad vehicle wheel performance. The work presented in this report was performed by Technology & Management Systems, Inc. (TMS), under Contract No. DTRS-57-93-C-00040, Technical Task Directive No. 2, from the Volpe National Transportation Systems Center (Volpe Center), U.S. Department of Transportation, Cambridge, MA. Dr. Phani K. Raj was the Project Manager at TMS. The project team included Dr. Keith E. Crowe, who performed a significant part of the technical work, and Ms. Tamara L. DeGray, who helped in the organization and preparation of the report.

The work reported here involves the application of heat transfer principles to model the so-called "rail chill" effect. When a rail vehicle wheel is heated by friction braking, the rim temperature tends to rise at a greater or lesser rate depending upon the relative rates of heat generation and heat loss. Heat can be lost from the wheel via radiation from the hot surfaces, convection into the surrounding air stream created by the vehicle motion, conduction into the brake shoe, or conduction into the rail through the wheel-rail contact area. The last pathway is called the rail chill effect.

The second report in this series documented a heat transfer finite element model of a non-standard passenger vehicle wheel subjected to transient conditions of stop braking. That model, calibrated from field test results summarized in the fourth report of the series, suggested that only a small percentage of the generated heat was being conducted away through the rail. This result did not agree with the rail chill effects reported from earlier tests conducted by the Association of American Railroads (AAR). The AAR tests were simulations of freight car wheel drag braking conducted on a dynamometer. In the present report, the apparent disagreement is resolved as a difference in the definitions of "rail chill," and the two bodies of research are shown to be consistent.

The TMS team acknowledges with gratitude the illuminating technical discussions with Dr. Oscar Orringer of the Volpe Center. Dr. Orringer, who was the COTR on this project, provided valuable technical direction. We are also indebted to Mr. Jeffrey Gordon and Ms. Yim Har Tang of the Structures and Dynamics Division for their draft report reviews and informative comments.

METRIC/ENGLISH CONVERSION FACTORS

ENGLISH TO METRIC

LENGTH (APPROXIMATE)

1 inch (in) = 2.5 centimeters (cm)
1 foot (ft) = 30 centimeters (cm)
1 yard (yd) = 0.9 meter (m)
1 mile (mi) = 1.6 kilometers (km)

AREA (APPROXIMATE)

1 square inch (sq in, in^2) = 6.5 square centimeters (cm^2)
1 square foot (sq ft, ft^2) = 0.09 square meter (m^2)
1 square yard (sq yd, yd^2) = 0.8 square meter (m^2)
1 square mile (sq mi, mi^2) = 2.6 square kilometers (km^2)
1 acre = 0.4 hectare (ha) = 4,000 square meters (m^2)

MASS - WEIGHT (APPROXIMATE)

1 ounce (oz) = 28 grams (gm)
1 pound (lb) = .45 kilogram (kg)
1 short ton = 2,000 pounds (lb) = 0.9 tonne (t)

VOLUME (APPROXIMATE)

1 teaspoon (tsp) = 5 milliliters (ml)
1 tablespoon (tbsp) = 15 milliliters (ml)
1 fluid ounce (fl oz) = 30 milliliters (ml)
1 cup (c) = 0.24 liter (l)
1 pint (pt) = 0.47 liter (l)
1 quart (qt) = 0.96 liter (l)
1 gallon (gal) = 3.8 liters (l)
1 cubic foot (cu ft, ft^3) = 0.03 cubic meter (m^3)
1 cubic yard (cu yd, yd^3) = 0.76 cubic meter (m^3)

TEMPERATURE (EXACT)

°C=5/9(°F - 32)

METRIC TO ENGLISH

LENGTH (APPROXIMATE)

1 millimeter (mm) = 0.04 inch (in)
1 centimeter (cm) = 0.4 inch (in)
1 meter (m) = 3.3 feet (ft)
1 meter (m) = 1.1 yards (yd)
1 kilometer (km) = 0.6 mile (mi)

AREA (APPROXIMATE)

1 square centimeter (cm^2) = 0.16 square inch (sq in, in^2)
1 square meter (m^2) = 1.2 square yards (sq yd, yd^2)
1 square kilometer (km^2) = 0.4 square mile (sq mi, mi^2)
10,000 square meters (m^2) = 1 hectare (ha) = 2.5 acres

MASS - WEIGHT (APPROXIMATE)

1 gram (gm) = 0.036 ounce (oz)
1 kilogram (kg) = 2.2 pounds (lb)
1 tonne (t) = 1,000 kilograms (kg) = 1.1 short tons

VOLUME (APPROXIMATE)

1 milliliter (ml) = 0.03 fluid ounce (fl oz)
1 liter (l) = 2.1 pints (pt)
1 liter (l) = 1.06 quarts (qt)
1 liter (l) = 0.26 gallon (gal)
1 cubic meter (m^3) = 36 cubic feet (cu ft, ft^3)
1 cubic meter (m^3) = 1.3 cubic yards (cu yd, yd^3)

TEMPERATURE (EXACT)

°F=9/5(°C) + 32

QUICK INCH-CENTIMETER LENGTH CONVERSION

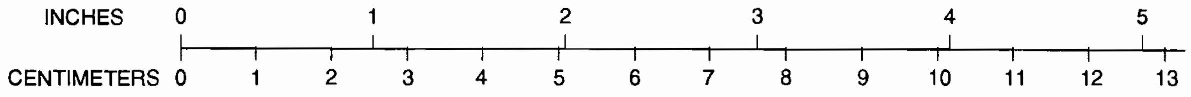

QUICK FAHRENHEIT-CELSIUS TEMPERATURE CONVERSION

°F	-40°	-22°	-4°	14°	32°	50°	68°	86°	104°	122°	140°	158°	176°	194°	212°
°C	-40°	-30°	-20°	-10°	0°	10°	20°	30°	40°	50°	60°	70°	80°	90°	100°

For more exact and or other conversion factors, see NIST Miscellaneous Publication 286, Units of Weights and Measures. Price $2.50. SD Catalog No. C13 10286.

Updated 8/1/96

TABLE OF CONTENTS

Section **Page**

1. INTRODUCTION 1-1

    1.1 Background 1-1
    1.2 The Rail Chill Effect 1-2
    1.3 Literature Review 1-2
    1.4 Objectives 1-3
    1.5 Report Organization 1-3

2. RAIL CHILL HEAT TRANSFER MODEL 2-1

    2.1 Model Assumptions 2-1
    2.2 Model Details 2-1

        2.2.1 Contact Area 2-1
        2.2.2 Interfacial Heat Transfer 2-3
        2.2.3 Thermal Boundary Layer Resistance 2-4
        2.2.4 Heat Generation Rate 2-5
        2.2.5 Rail Chill Effectiveness 2-6
        2.2.6 Rail Chill Effect during Stop Braking 2-8
        2.2.7 Contact Heat Transfer Coefficient (h_c) 2-8
        2.2.8 Rail Chill Effect during Drag Braking 2-11

3. APPLICATION OF THE RAIL CHILL MODEL 3-1

    3.1 Comparison of the Rail Chill Model to the Association of American Railroads (AAR) Data 3-1
    3.2 Energy Balance Model to Compute η^* 3-1
    3.3 Parametric Dependence of the Rail Chill Effect 3-5

4. DISCUSSIONS AND CONCLUSIONS 4-1

    4.1 Discussions 4-1
    4.2 Conclusions 4-2

APPENDIX A. Determination of Wheel-Rail Contact Area, A_c A-1
APPENDIX B. Parametric Dependence of Rail Chill B-1
APPENDIX C. Evaluation of Mean Rail Chill Effectiveness Factor C-1
APPENDIX D. Longitudinal Rail Conduction Effects D-1
APPENDIX E. Relation between Wheel Temperature and Brake Power Input E-1

NOMENCLATURE N-1

REFERENCES R-1

LIST OF FIGURES

Figure **Page**

2-1. Schematic Representation of Heat Generation Due to Braking and Cooling from the Rail Chill Effect 2-2

3-1. Description of Wheel Heat Transfer Experiments at AAR 3-2

3-2. Measured Tread Temperature and Calculated Rail Chill Effectiveness vs. Drag Brake Input Power from AAR Tests 3-3

3-3. Rail Chill Effectiveness vs. Correlation Parameter for Stop Braking and Drag Braking 3-7

LIST OF TABLES

Table **Page**

2-1. Rail Chill Effectiveness for Different Braking Conditions 2-9

2-2. Rail Chill Effectiveness for Two Drag Braking Examples 2-11

3-1. Comparison of Rail Chill Results for Several Cases in AAR Tests 3-4

1. INTRODUCTION

1.1 BACKGROUND

The application of tread brakes to slow down the speed of a train results in the generation of heat at the brake shoe-wheel interface. The rate of heat liberation (or, alternately, the power dissipated) at the brake shoe depends on the rate at which the kinetic energy of the train is decreased. That is, the heat production rate at each brake shoe-wheel interface depends on the mass of the train, its speed, the magnitude of deceleration, and the number of wheels on which braking is effected.

There are two types of braking phenomena, depending on the intent of brake application. The first type is "stop braking," in which the initial speed of the train is reduced substantially, or the train is brought to rest. This type of braking is used for stopping the train either at scheduled stops or in an emergency. The second type of braking is "drag braking." In this case, a potential increase in train speed is arrested by applying the brake to the train wheel at about a constant pressure for a relatively long duration of time, for example, while descending a long grade. The intent of this type of braking is to maintain the train speed at a specified value (under conditions when otherwise the train may have accelerated).

In the case of stop braking, the rate of heat generation at the brake shoe-wheel interface is high because of the substantial train kinetic energy that has to be dissipated in a relatively short time (a few minutes). Therefore, the temperature of brake shoe and wheel rim increases rapidly, while the other parts of the brake and the wheel are still at relatively lower temperature. Stop braking is a short-time phenomenon; i.e., the wheel temperature increases rapidly during brake shoe contact and decreases due to ambient cooling when the shoe is disengaged from the wheel. In general, stop braking may involve repeated application and disengagement of the brake shoe with the wheel.

The temperature variation of the wheel rim in drag braking is different from that in stop braking. In general, the power dissipation levels in drag braking are lower than in stop braking; however, the duration over which the brake shoe will be in contact with the wheel is longer. In this situation, the temperature of the wheel rim reaches a maximum value and then remains essentially constant. The highest wheel temperature in drag braking is generally lower in value than in the case of stop braking because of the lower magnitude of power dissipation in drag braking. The peak temperature attained by the wheel rim is determined by the rate of heat generation at the brake shoe and the rate of convective and radiative cooling of the wheel. Any additional wheel cooling results in reducing the peak temperature value. One such additional cooling "mechanism" is the transfer of heat between the wheel and the rail with which the wheel is in contact. The evaluation of the effectiveness of this cooling path is the subject of this report.

1.2 THE RAIL CHILL EFFECT

A hot wheel in contact with the rail on which it is rolling transfers heat to the rail by conduction. In general, the rail is at a significantly lower temperature compared to a wheel rim heated by the brake shoe friction. This type of cooling of the wheel is termed the "rail chill" to distinguish this cooling mechanism from other modes of wheel cooling (natural convection, forced convection, and radiation). The mean rate at which heat is transferred between the wheel and the rail will be dependent on the temperature difference, area of wheel-rail contact, contact thermal resistance, and the duration of contact.[1] The fraction of the heat generated at the brake shoe-wheel interface that is removed through the rail is termed the "rail chill efficiency." This report provides details of calculation of the rail chill efficiency for both drag braking and stop braking under different train operating conditions.

The importance of rail chill lies in the fact that it provides an additional wheel cooling mechanism. Hence, any laboratory study on wheel thermal stresses (dependent on both the temperature and temperature gradients in the wheel rim) should address the simulation of the rail chill mechanism if proper modeling of the wheel conditions are to be fulfilled. The inclusion or exclusion of rail chill in laboratory studies will depend on the magnitude of rail chill *vis-a-vis* the power dissipation (i.e., the value of rail chill efficiency).

1.3 LITERATURE REVIEW

We are not aware of any study that has evaluated the phenomenon of rail chill using the principles of heat transfer. The wheel thermal damage study reported by Stone and Carpenter (1994) has recognized the importance of rail chill. In this study, the researchers measured peak temperature in wheel rims under different brake power dissipation levels on a dynamometer. The rim temperature was also measured in the presence of a large wheel in contact with the train wheel. The large wheel represented the "cooler rail" and the contact wheel temperature was maintained at levels far lower than the train wheel temperature. Also measured after each test were the nature and magnitude of thermally induced stresses in the train wheel.

Stone and Moyar (1989) report experimental values of rail chill effectiveness (defined as the fraction of brake power dissipation transferred as heat to the rail) of 15.2% and use this result to compute thermal stresses in the wheel tread. They suggested that the stresses induced by the transient rail heat transfer may be sufficient to initiate surface cracks in the wheel rim. In addition, they hypothesized that the rapid cooling effect of rail chill could potentially cause microstructural changes in the wheel material, depending on the temperatures attained during braking. Thus, although the rail chill effect may be beneficial from the standpoint of reducing the wheel temperature, the rapid and localized tread cooling may be detrimental.

---

[1] The concept of "duration of contact" between a rolling wheel and the rail on which it is rolling requires an explanation. When a wheel rolls on a rail, elastic deformation of both bodies results in a translating area of contact. The "duration of contact" is defined as the time duration from the moment the moving contact area first comes in contact with a given rail crown point to when the contact area does not contain the specified rail crown point. Obviously, this contact time depends on the translational velocity of the wheel and the length of contact area along the rail.

It is found from the test results presented by Stone and Carpenter (1994), and Opinsky and Joerms (1986), that rail chill efficiency varies between 20 and 90% for drag braking. These test results and their implications are discussed in this report. A number of questions related to the rail chill effect remain unresolved.

This study was initiated to study, model, and analyze the rail chill effect. It is hoped that the results of the study will be useful in designing wheel stress assessment tests and also in analyzing results from different tests on a rational basis.

1.4 OBJECTIVES

The objectives of this study are to:

- model the phenomenon of heat transfer between a hot railcar wheel and a cooler rail on which the wheel is rolling;
- determine the dependence of rail chill on the controlling parameters such as railcar weight and speed; and
- evaluate the importance of the rail chill effect in the overall cooling mechanisms of a wheel heated by braking.

1.5 REPORT ORGANIZATION

A rail chill heat transfer model is discussed and developed in Section 2. The descriptions include the calculation of the wheel-rail contact area (§2.2.1), interfacial heat transfer (§2.2.2 and §2.2.3), heat generation rate at the brake shoe-wheel interface (§2.2.4), and rail chill effectiveness (§2.2.5). Both drag braking and stop braking are discussed. Also elaborated in this section are the contact resistance effects and proper consideration of rail chill efficiency. Two case study results are presented.

In Section 3, the rail chill analysis is applied to several braking scenarios tested in laboratory experiments. The test data and results from the model presented in this report are compared. Also, the scaling relationship between the rail chill and controlling parameters is established.

The discussion of the results is provided in Section 4. This includes the dependence of "rail chill efficiency" on model assumptions and on the numerical values of the influencing parameters. The conclusions from the study are also indicated in Section 4.

2. RAIL CHILL HEAT TRANSFER MODEL

The physical situation of heat generation at the brake shoe-wheel interface and heat transfer to the rail is shown schematically in Figure 2-1. Heat is generated due to the application of the brake. The heat generation rate is represented by $\dot{Q}_{gen}$. The rate at which heat is conducted to the rail is represented by $\dot{Q}_{rail}$. The determination of the value of $\dot{Q}_{rail}$ for given $\dot{Q}_{gen}$ (when other parameters are specified) is indicated in the model discussed below.

2.1 MODEL ASSUMPTIONS

In deriving the equations below, the following assumption are made. The implications of these assumptions on the final results are discussed in Section 4.

1. The contact area for the transfer of heat between the wheel and the rail is elliptical.

2. The thermal contact resistance between the wheel and the rail is negligible (in fact, in our model this resistance is set to zero).

3. The heat transfer is one-dimensional and in the rail depth direction. That is, heat conduction in the rail longitudinal direction and rail gage direction are negligible. Appendix D discusses longitudinal conduction effects and provides justification for this assumption. Similar arguments hold for conduction in the rail gage direction.

4. The finite thicknesses of the wheel rim and the rail (in the vertical direction) do not affect the heat transfer rates across the interface.

5. The thermal properties of materials are not dependent on the temperature and are assumed to be the same for wheel and rail.

6. Radiation and convective heat losses from the rail sides are not important (and, hence, are neglected).

2.2 MODEL DETAILS

2.2.1 Contact Area

The area of contact between two solid bodies in loaded contact may be estimated from elasticity theory according to the theory of Hertz. Timoshenko and Goodier (1951) give a thorough treatment; however, only the key results will be given here.

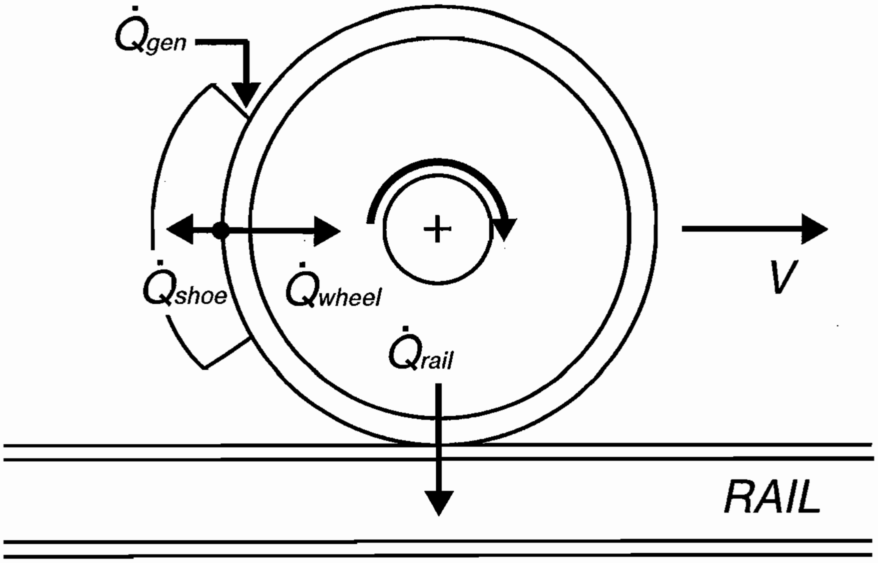

Figure 2-1. **Schematic Representation of Heat Generation Due to Braking and Cooling from the Rail Chill Effect**

The contact between the wheel and rail may be modeled as two mutually perpendicular cylinders of different radii loaded against one another with a force of magnitude *P*. It is shown that the area of contact is bounded by an ellipse whose major and minor axis lengths are a function of material properties, loading, and radius of each cylindrical member.[1] Using the properties of steel and radii of curvature of 0.3 m (12 in.) and 0.4 m (16 in.), respectively, for the rail and wheel, the semi-axes for the elliptical contact area are computed to be:

$$a = 0.0146P^{1/3} \qquad (2\text{-}1a)$$

$$b = 0.0122P^{1/3} \qquad (2\text{-}1b)$$

---

[1] Details of the equations are provided in Appendix A.

Here, the single wheel axle load, P, is in Newtons and the semi-axes lengths (a, b) are in cm. In this case, the major axis, a, is parallel to the rail. The area of contact (the ellipse) is found from

$$A_c = \pi\ a\ b = 5.595 \times 10^{-4}\ P^{2/3} \tag{2-2}$$

As can be seen from the above equation, the contact area varies with ⅔ power of the wheel load. For example, in the case of a railcar weighing 131.5 tons (263,000 lbs.) and having 8 wheels, the load on each wheel is 146.3 kN. At this load, the contact area is 1.55 cm^2. On the other hand, for a car of weight 70 tons (140,000 lbs.) the contact area is 1.02 cm^2.

2.2.2 Interfacial Heat Transfer

The interfacial heat transfer rate is modeled with the equation

$$\dot{Q}_{rail} = h\ A_c \left(T_{wheel} - T_{rail}\right) \tag{2-3}$$

where

h = Effective heat transfer coefficient (which includes the effects of contact resistance and thermal boundary layer in the two bodies)
A_c = Contact area
T_{wheel} = Temperature of wheel (assumed to be constant)
T_{rail} = Temperature of rail (assumed to be constant)

The value of h, in general, is dependent on the duration of contact, the contact surface roughness, and load. It can be assumed without loss of generality that the overall resistance to heat transfer at the interface (R_{int}) is the sum of contact resistance (R_c) and "resistance" due to the development of thermal boundary layers (R_{bl}) in both contacting bodies. That is,

$$R_{int} = R_c + R_{bl}(t) \tag{2-4}$$

in which the time dependence of boundary layer resistance is indicated. Equation 2-4 is recast in terms of heat transfer coefficients as

$$h_{int} = \left[\frac{1}{h_c} + \frac{1}{h_{bl}(t)} \right]^{-1} \tag{2-5}$$

The cooling effect of a rail is at maximum if the contact resistance (R_c) is zero. While this is not realistic, we can estimate the maximum rail chill effect and determine if it is significant or not. It is with this perspective (see assumption 2) that we treat the interface heat transfer problem as one with no contact resistance. In this case, the evaluation of interface heat transfer reduces to the evaluation of the thermal boundary layer resistance.

2.2.3 Thermal Boundary Layer Resistance

It is assumed that at a given instant (t = 0) the hot wheel at temperature T_{wheel} and the rail at temperature T_{rail} are brought together with perfect thermal communication between them. The time dependent, one dimensional heat transfer flux is given by

$$\dot{q}''(t) = \frac{k\ \Delta T}{2\sqrt{\pi \alpha t}} \tag{2-6}$$

Where $\Delta T = (T_{wheel} - T_{rail})$. The heat flux decays rapidly with time. The average heat flux over the contact time, t_c, is then

$$\overline{\dot{q}''} = \frac{k\ \Delta T}{\sqrt{\pi \alpha t_c}} \tag{2-7}$$

The boundary layer coefficient, h_{bl}, is then

$$h_{bl} = \frac{\overline{\dot{q}''}}{\Delta T} = \frac{k}{\sqrt{\pi \alpha t_c}} \tag{2-8}$$

It is to be noted that the boundary layer heat transfer coefficient (h_{bl}) depends only on the material thermal properties and contact time, t_c.

The mean interfacial heat transfer rate over time t_c can then be written as

$$\dot{Q}_{rail} = A_c \frac{k\left(T_{wheel} - T_{rail}\right)}{\sqrt{\pi \alpha t_c}} \tag{2-9}$$

In the case of a wheel rolling on a rail, a given point on the wheel is in contact with the rail only while the given point is inside the (moving) contact area. That is,

$$t_c = \frac{\ell}{V} \tag{2-10}$$

where

ℓ = a characteristic length of contact area in the rail longitudinal direction
V = linear translational speed of the wheel

We postulate that ℓ be set equal to an average length as follows:

$$\ell = \frac{\mathit{Area\ of\ Elliptical\ Contact}}{\mathit{Length\ of\ Minor\ Axis}} = \frac{\pi}{2}\, a \tag{2-11}$$

2.2.4 Heat Generation Rate

The heat generation rate at each wheel due to frictional braking at any instant of time after the application of the brake is[2]

$$\dot{Q}_{gen} = \left[\frac{m}{N_{wheel}}\right] a_d\, V(t) \tag{2-12}$$

where

m = Mass of each car
N_{wheel} = Number of wheels per car
a_d = Deceleration due to braking
$V(t)$ = Velocity of the car at any instant

---

[2] Neglecting the aerodynamic drag effects and rolling resistances.

2.2.5 Rail Chill Effectiveness

As indicated earlier, the rail chill efficiency can be defined as

$$\mathit{Rail\ Chill\ Efficiency} = \frac{\mathit{Rate\ of\ heat\ transfer\ to\ the\ rail}}{\mathit{Power\ dissipation\ at\ the\ brake\ shoe\text{-}wheel\ interface}} \tag{2-13}$$

In the above equation, both the numerator and the denominator on the right hand side are evaluated at the same time instant. While the above definition is very precise, it is very difficult to evaluate both parameters at the same time. This is because, during the initial stages, a significant fraction of heat generated at the brake goes to heat the wheel, and at the same time the wheel is being cooled by convective cooling. To calculate the rate of heat transfer to the rail, one needs the wheel rim temperature, which is a rapidly changing function of time. The temperature-time history of the wheel rim can be calculated, provided the area for cooling and the convective heat transfer coefficient are known (these are difficult to specify accurately). Hence, the instantaneous rail chill efficiency defined in Equation 2-13 becomes difficult to calculate. However, when the wheel temperature has reached its maximum, the heat loss to the ambient environment (including the rail chill) is roughly balanced by heat input to the wheel at the brake. The rail chill efficiency can then be defined using Equation 2-13.

There is a second philosophical difficulty in using Equation 2-13. Normally, the efficiency of a process is defined on the basis of a cause-and-effect phenomenon (cause — heat is transferred to the wheel; effect — heat is extracted at the wheel-rail interface) so that the effect phenomenon can be studied when the causal factors change. In the definition of Equation 2-13, when the dissipation power magnitude changes, not all of the change goes to the wheel; a part (perhaps not a constant part) of the heat generated goes to the brake shoe and its components. Hence, a more rational definition of rail chill efficiency is

$$\eta(t) = \frac{\mathit{rate\ of\ heat\ loss\ to\ the\ rail}\ (\dot{Q}_{rail})}{\mathit{rate\ of\ heat\ input\ to\ the\ wheel\ at\ the\ brake}\ (\dot{Q}_{wheel})} \tag{2-14}$$

and

$$\eta^* = \frac{\dot{Q}_{rail}\left(T_{wheel} = T_{wheel}^{\max}\right)}{\dot{Q}_{wheel}\left(T_{wheel} = T_{wheel}^{\max}\right)} \tag{2-15}$$

where

η^* = Effectiveness (or efficiency) of rail chill at the instant when the wheel rim temperature is at its maximum

$\dot{Q}_{rail}\left(T_{wheel} = T_{wheel}^{\max}\right)$ = Heat transfer rate into the rail at the time when the wheel temperature is at its maximum

$\dot{Q}_{wheel}\left(T_{wheel} = T_{wheel}^{\max}\right)$ = Heat input rate into the wheel when the wheel temperature is at its maximum.

Since, in a given train operation situation, the value of only the power dissipation is known, we make a (justifiable) assumption that only 90% of heat generated goes into the wheel. That is,

$$\dot{Q}_{wheel} = 0.9\ \dot{Q}_{gen} \tag{2-16}$$

Note, however, that because the wheel is rolling and in contact with different parts of the rail at different times, the value of $\dot{Q}_{rail}$ is to be calculated as the product of average value of heat flux into the rail over the period of contact and the area of contact (i.e., using Equation 2-9). These equations are applied to specific cases to determine the effectiveness of the rail chill phenomenon.

The average rail chill efficiency over the duration of wheel rim heating from ambient temperature to its maximum temperature can be calculated, if the temperature-time history of the wheel is known. This average efficiency can be written as follows:

$$\bar{\eta} = \frac{\int_o^{t(T_{\max})} \dot{Q}_{rail}\ dt}{\int_o^{t(T_{\max})} \dot{Q}_{wheel}\ dt} \tag{2-17}$$

where $t(T_{\max})$ is the time when the rim temperature is at its maximum. This expression indicates that average rail chill efficiency is the ratio of the total thermal energy released to the rail and the total heat input to the wheel over the time, t. This quantity cannot be evaluated as readily as η^* since its calculation requires knowledge of the rim temperature as a function of time, and the time of maximum temperature, $t(T_{\max})$. However, because of its physically based importance, it is used in this study in addition to η^*. Estimation of $\bar{\eta}$ requires some additional modeling assumptions. The details can be found in Appendix C.

2.2.6 Rail Chill Effect during Stop Braking

Stop braking is said to occur when the brakes are applied on a moving wheel to reduce the velocity of the car from a high value to a low value (or zero). In this case, the velocity is continuously decreasing and, in general, the duration over which the brakes are active is relatively short. However, the rate of deceleration will be high.

It is found from both numerical simulations and experimental data that the wheel temperature reaches a maximum at about the midway point in the braking event (i.e., when the velocity of the vehicle is about one-half of the initial high speed under constant deceleration). Under these conditions, in a stop braking event, the temperature of the wheel rim attains a maximum value when the energy dissipation (at the brake-wheel interface) is about one-half of the peak dissipation rate.

Table 2-1 shows the results obtained for stop braking for three typical sets of parameters (car weight, deceleration rate, and initial velocity). Details of these braking scenarios are reported by Tang, et al. (1993). In each case, the heat input rate into the wheel is calculated as 90% of the power dissipation rate at a time when the wheel rim temperature is at its maximum. The first part of the table provides the rail chill effectiveness results when no thermal contact resistance is assumed at the wheel-rail interface.

The results indicate that the overall rail chill effect is between 12% and 16%. This means that rail chill accounts for 12 to 16% of the total cooling (which includes radiation and convection components) at the time when the wheel tread temperature is at its maximum. These effectiveness values will be smaller when the interfacial thermal contact resistance is taken into consideration. This phenomenon is discussed next.

2.2.7 Contact Heat Transfer Coefficient (h_c)

It can be argued that the presence of thermal contact resistance decreases the rail chill effectiveness. As demonstrated in the examples in the previous section, the magnitude of the overall rail chill effectiveness is small. Therefore, it may not be necessary for the contact resistance value to be determined with a great degree of accuracy.

Our review of literature (Rohsenow and Hartnett 1973; Fenech and Rohsenow 1963) on contact resistance indicates that the interfacial pressures studied were under 80 MN/m^2 (10,000 psi), whereas the axle loads on a typical railcar wheel are in the neighborhood of 700 MN/m^2 (100,000 psi). Hence, the data presented in the literature on heat transfer contact resistance may not be directly applicable to the problem under consideration. For example, the values for contact heat transfer coefficients (h_c) reported in the literature (Rohsenow and Hartnett 1973) vary between 1700 W/m^2 K to 10,000 W/m^2 K for interfacial pressures up to 7 MN/m^2 (1,000 psi). No data are available at 700 MN/m^2.

Table 2-1. Rail Chill Effectiveness for Different Braking Conditions

			Case Study Details†		
Item	Parameters	Units	Freight Car Braking	Passenger Car Braking	Passenger Car Braking
1	Total Car Weight	kN	1170	623	543
2	Number of Wheels per Car		8	8	8
3	Initial Speed Before Braking	m/s	36	45	39
4	Deceleration Rate	m/s^2	0.45	0.89	0.86
5	Peak Wheel Rim Temperature	C	427	514	382
6	Ambient Temperature	C	32	10	10
7a	Maximum Heat Input Rate at Each Wheel	kW	215	286	209
7b	Heat Input Rate at Peak Temp of Wheel Rim	kW	107	154	96
8	Wheel-Rail Contact Area, A_c	cm^2	1.51	0.99	0.9
9	Contact time (t_c) for heat transfer coefficient calculation	s	6.7×10^{-4}	4.0×10^{-4}	5.2×10^{-4}
Assuming Zero Contact Resistance					
10	Mean Interface Heat Transfer Rate ($\dot{Q}_{rail}$)	kW	17	19	11
11a	Rail Chill Effectiveness Factor, η^*	%	16	12	12
11b	Average Rail Chill Effectiveness Factor, $\bar{\eta}$	%	6.1	4.6	4.6
With Contact Resistance Included					
12	Mean Interface Heat Transfer Rate ($\dot{Q}_{rail}$)	kW	10	8.9	5.1
13a	Rail Chill Effectiveness Factor, η^*	%	9.5	5.8	5.3
13b	Rail Chill Effectiveness Factor, $\bar{\eta}$	%	3.6	2.2	2

†See Tang, et al. (1993)

Fenech and Rohsenow (1963) have modeled the thermal contact resistance problem and have successfully compared test data with model results. It was found that the heat transfer contact area is smaller than the nominal contact area calculated using the structural contact problem (Equation 2-2). The heat transfer contact area, A_h, is related to the yield strength (σ_y) of the softer of the contacting materials by the equation:

$$A_h = \frac{P}{3\sigma_y} \tag{2-18}$$

where P is the interfacial load.[3]

If the area A_h is used (instead of A_c) in interfacial heat transfer calculations, the contact resistance is effectively taken into consideration. Therefore, the actual interfacial heat transfer rate can be written as (see Equation 2-9)

$$\underset{(with\ contact\ resistance)}{\dot{Q}_{rail}} = A_h \frac{k\left(T_{wheel} - T_{rail}\right)}{\sqrt{\pi \alpha t_c}} \tag{2-19}$$

The overall heat transfer coefficient, h_{int}, defined with the contact area, A_c, can then be determined from the equation

$$h_{int} = \frac{\dot{Q}_{rail}}{\left(T_{wheel} - T_{rail}\right) A_c} \tag{2-20}$$

Table 2-1 also shows the results for the rail chill effectiveness when the contact resistance is also considered as indicated above. It is seen that, with the inclusion of the effects of thermal contact resistance, the rail chill effectiveness decreases by almost one-half the value in the absence of thermal resistance at the interface. However, in either case the absolute value of the effectiveness is small, indicating that only a small fraction of the heat generated at the brake-wheel interface can be dissipated through the wheel-rail interface during stop braking.

---

[3] For a load of $P = (1170/8) = 146.3$ kN, the contact area, A_c, is calculated (Equation 2-2) to be 1.55 cm^2. With a material of $\sigma_y = 550$ MN/m^2 (80,000 psi), the calculated heat transfer area is $A_h = 0.9$ cm^2, which is about 57% of the structural contact area, A_c.

2.2.8 Rail Chill Effect during Drag Braking

Drag braking is practiced in slowing freight and other trains when the train is traveling downhill. The objective in drag braking is to maintain a constant speed. Therefore, drag braking tends to have the following characteristics: long duration of sustained braking; relatively low power dissipation levels; and relatively lower maximum wheel rim temperatures.

Table 2-2 shows the effect of drag braking on the rail chill effectiveness. In calculating the results presented in Table 2-2, we have used wheel rim temperature values calculated by the Association of American Railroads (AAR) (Opinsky and Joerms) for the case of 21.8 kW heat dissipation rate per wheel for a 20-minute duration. Note, however, the heat input *to the wheel* shown in Table 2-2 is 90% of the 21.8 kW (19.6 kW) in accord with the assumption stated in Equation 2-16.

Table 2-2. Rail Chill Effectiveness for Two Drag Braking Examples

Item	Parameter	Units	Case Study Details†	
			Freight Car	Passenger Car
1	Total Car Weight	kN	1170	623
2	Number of Wheels per Car		8	8
3	Constant Speed	m/s	36	36
4	Peak Wheel Rim Temperature	C	296	296
5	Ambient Temperature	C	10	10
6	Maximum Heat Input at Each Wheel ($\dot{Q}_{wheel}$)	kW	19.6	19.6
7	Wheel-Rail Contact Area	cm^2	1.51	0.99
8	Contact Time for Heat Transfer Coefficient Calculation	s	3.3×10^{-4}	2.7×10^{-4}
Assuming Zero Contact Resistance				
9	Mean Interface Heat Transfer Rate	kW	17.8	13.0
10	Rail Chill Effectiveness Factor, η^*	%	91	66
With Contact Resistance Included				
11	Mean Interface Heat Transfer Rate	kW	10.4	6.2
12	Rail Chill Effectiveness Factor, η^*	%	53	32

†See Opinsky and Joerms (1986)

It is seen in Table 2-2 that the rail chill effectiveness during these drag braking examples is substantially higher than during stop braking. When contact resistance is neglected, the effectiveness is so large it becomes the dominant heat dissipation mechanism. The reasons for the substantial change are the lower heat generation rate (which appears in the denominator of the rail chill effectiveness factor) and the higher train speed. The effective interfacial heat transfer coefficient is larger, since the contact time is shorter. These examples have used 36 m/s (80 mph) in the calculation, but actual drag braking involves speeds of less than 18 m/s (40 mph). All else being constant, Equation 2-9 indicates that the rail heat transfer rate (and thus rail chill effectiveness) depends on contact time, $t_c^{-\frac{1}{2}}$. Therefore, rail chill effectiveness will depend on $V^{\frac{1}{2}}$. For example, the rail chill effectiveness for a train traveling 40 mph will be only about 70% of that for an 80 mph train, all else being constant.

The results indicate that the rail heat transfer rate cannot be neglected, so it is advisable to consider the rail chill effect in models that predict wheel rim temperature during drag braking. In the next section, the model developed above is applied to the conditions of the laboratory experiments where drag braking with and without rail heat transfer was simulated (Stone and Carpenter 1994). The experimental results are compared with predictions from the model developed in this section.

3. APPLICATION OF THE RAIL CHILL MODEL

In this section, we compare the results of Section 2 to the only known experimental data where rail heat transfer has been simulated in tests. In addition, the dependence of the rail chill effectiveness factor on the controlling parameters is derived and presented in a concise and practical way.

3.1 COMPARISON OF THE RAIL CHILL MODEL TO THE ASSOCIATION OF AMERICAN RAILROADS (AAR) DATA

To this point, the rail chill model has been used to estimate the heat transfer to the rail for given braking scenarios. It is difficult, in practice, to evaluate the rail chill model, since measurements are not routinely done under actual train operating conditions. However, work performed at the Research and Test Department of the AAR in Chicago (Stone and Carpenter 1994) allows indirect comparison of the present results with measurements.

In the work of Stone and Carpenter, wheel temperatures were measured under controlled thermal loading conditions, where a fixed brake power input on a single constant velocity wheel (of diameter between 28 and 38 inches) was employed. The steady-state tread temperature was measured with and without the presence of a contacting "rail wheel." This 110-inch-diameter steel wheel, in contact with 12000 lbs load, was employed to simulate the heat transfer interaction of the rail. Figure 3-1 illustrates the experimental description.

Figure 3-2 shows measured steady-state tread temperature (with wheel-rail contact) and rail chill effectiveness calculated using the model described in the last section, as a function of brake power input for a CE-28 (28-inch-diameter) wheel. The tread temperature follows a straight line with a simple correlation provided. For an input power of 44.8 kW (60 hp), the tread temperature *without rail contact* is also shown. The rail chill effectiveness shows some dependence on the input power, but is nominally around 20%.

Table 3-1 provides further comparison of tread temperatures with and without rail contact for several of the AAR test cases. The table also compares η^* evaluated by the present model, an AAR estimate, and an energy balance model described next.

3.2 ENERGY BALANCE MODEL TO COMPUTE η^*

The large drop in tread temperature at 60 hp due to the presence of rail contact (see Table 3-1) implies that the rail chill effect is measurable. A first order estimate of η^* can be made based on this data. For simplicity, we will assume thermal radiation heat transfer can be neglected. We can justify this assumption in two ways. The tread temperature shown in Figure 3-2 indicates a linear (with offset) increase in temperature with increasing power input. Linear behavior is not expected if radiation is significant. Also, we might estimate radiation heat transfer compared to the convection mode. For the data point with the largest tread temperature ($T = 649\,^{\circ}\mathrm{C}$, 60 hp brake power, no wheel-rail contact), the upper limit on the total radiation heat transfer is about 6000 W (using 0.15 square meter radiant heat transfer area and unit emissivity). This is roughly 13% of the total power dissipation (60 hp). Thus, we will assume that thermal radiation heat transfer can be neglected. We proceed with a first order estimate of rail chill using this data.

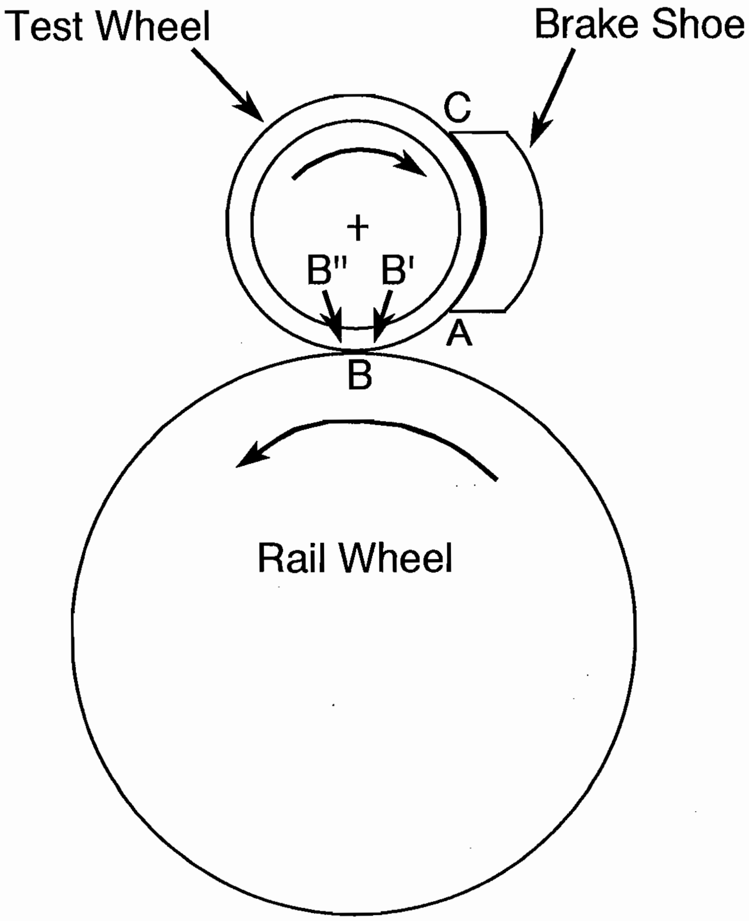

Figure 3-1. Description of Wheel Heat Transfer Experiments at AAR (Stone and Carpenter 1994)

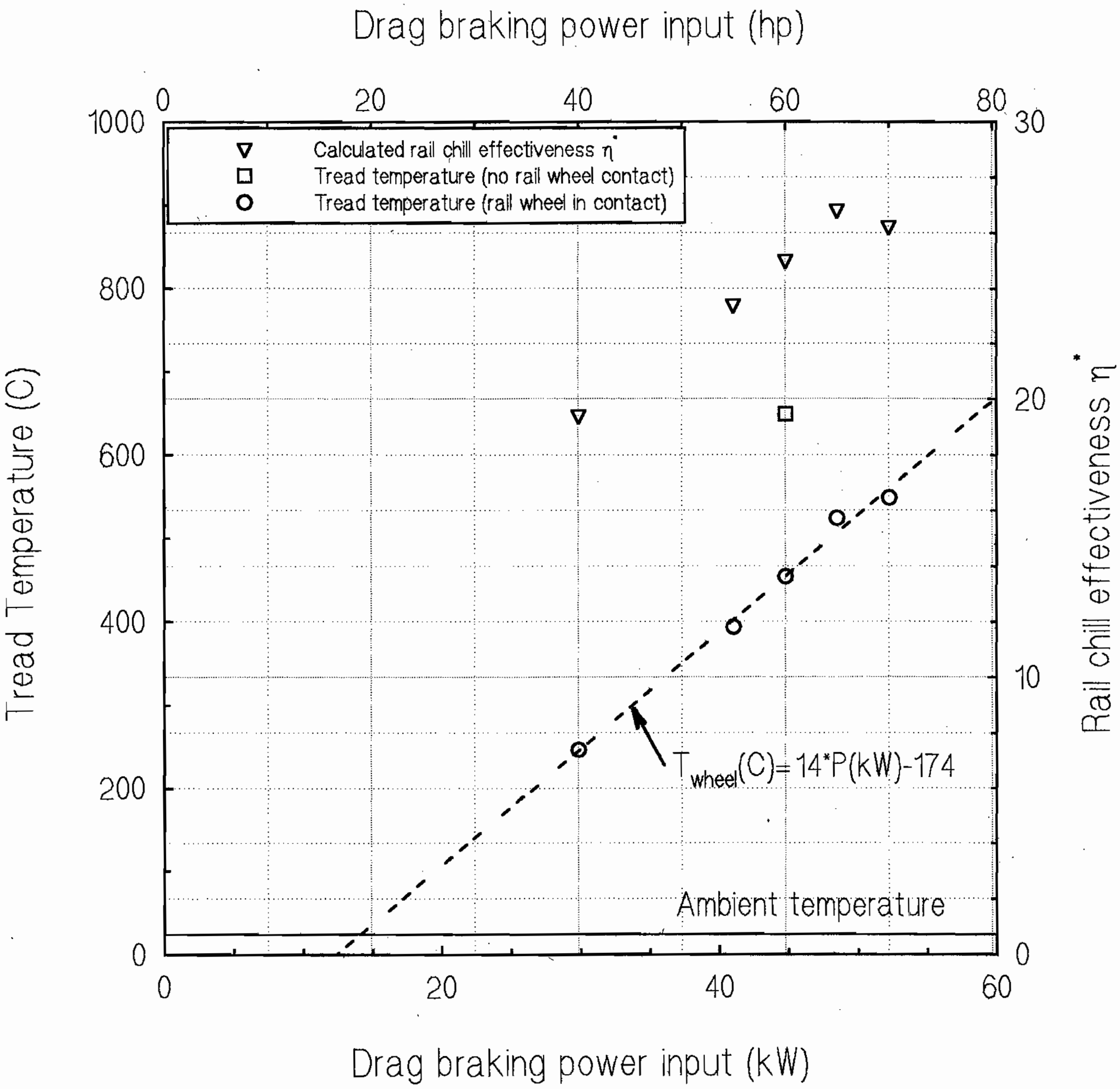

Figure 3-2. **Measured Tread Temperature and Calculated Rail Chill Effectiveness vs. Drag Brake Input Power from AAR Tests (Stone and Carpenter 1994)**

Table 3-1. **Comparison of Rail Chill Results for Several Cases in AAR Tests (Stone and Carpenter 1994)**

Test Conditions	Wheel Diameter	in	28	36	36	38
	Rim Thickness	in	1.44	1.62	0.88	1.12
	Wheel Peripheral Speed	mph	40	40	40	40
	Loading, P	lb	12000	12000	12000	12000
	Drag Brake Power	hp	60	60	60	70
	Brake Duration	hr	1.0	1.0	1.0	1.0
	Ambient temperature, T_a	°F	75	75	75	75
	Tread Temp. (rail contact)	°F	794	751	674	723
	Tread Temp. (no rail contact)	°F	1169	920	1051	958
Rail Chill Effectiveness η* at Wheel Rim Maximum Temperature	AAR Estimate*	%	18	18	18	18
	Energy Balance Model**	%	34	20	39	27
	Heat Transfer Model***	%	23	22	20	19

*means of estimation not reported by Stone and Carpenter
**See Section 3.2
***See Section 2

When there is no wheel-rail contact, the only mode of cooling is convective heat transfer. The steady state energy balance for this case is

$$\dot{Q}_{wheel_1} = (hA)_{conv} \left(T_{wheel_1} - T_a\right) \tag{3-1}$$

where $(hA)_{conv}$ is thermal conductance for convection, and T_a is the ambient air temperature, 75°F. For the case in which the rail wheel contacts the tread,

$$\dot{Q}_{wheel_2} = (hA)_{conv} \left(T_{wheel_2} - T_a\right) + \dot{Q}_{rail} \tag{3-2}$$

In this example, $\dot{Q}_{wheel_1} = \dot{Q}_{wheel_2} = \wp$, so that the rail heat transfer rate can be estimated from

$$\dot{Q}_{rail} = (hA)_{conv} \left(T_{wheel_1} - T_{wheel_2} \right) \qquad (3\text{-}3)$$

or

$$\eta^* = \frac{\dot{Q}_{rail}}{\dot{Q}_1} = \frac{\left(T_{wheel_1} - T_{wheel_2}\right)}{\left(T_{wheel_1} - T_a\right)} = 34\% \qquad (3\text{-}4)$$

Stone and Carpenter (1994) estimate a rail chill of 18% but do not give details on the means of estimation. Table 3-1 summarizes the computation of rail chill effectiveness for their data using their estimate, Equation 3-4, and the more detailed model developed in Section 2. For fixed speed and loading, it is expected that η^* should be fairly constant, yet the results, using Equation 3-4, indicate a variation factor of two. However, the agreement between the AAR estimate and the heat transfer model (developed in Section 2) is reasonable. We then conclude that the rail chill effectiveness under these loading and speed conditions is about 20%.

The only modes of significant heat loss from the wheel are forced convection and rail chill. Since these both depend linearly on tread temperature, the open circle points in Figure 3-2 should lie on a line intersecting ambient temperature at zero power. Equivalently, η^* is expected to be constant; however, it shows a seeming dependence on the power input. The reason for this behavior is unknown but might be explained by considering the fact that a thermal contact resistance exists at the brake shoe-wheel interface. As was pointed out in Section 2.2.7, the thermal contact resistance depends on the load, P. For a fixed wheel velocity, an increase in brake power requires a larger normal force between the brake shoe and wheel, which is accompanied by a decrease in the contact resistance. A model of the heat transfer at the brake shoe-wheel interface is presented in Appendix E to further explain this point.

3.3 PARAMETRIC DEPENDENCE OF THE RAIL CHILL EFFECT

An important result derived from this work is the dependence of the rail chill effect on the major parameters, namely, car weight, initial speed, and brake power. Using the model developed in Section 2, the effectiveness factor η^* was calculated using the simulated results for eight cases of stop braking (Tang, et al. 1993) in addition to experimental results from seven cases of simulated drag braking (Opinsky and Joerms 1986; Stone and Carpenter 1994). The results plotted in Figure 3-3 show η^* vs. the square root of car weight times initial (or constant) velocity. The parameter $(WV_i)^{1/2}$ is formed based on some first order scaling arguments for the dependence of η^* on the variables W and V. This is presented in detail in Appendix B.

Though there is some scatter, the straight line fit for stop braking validates the linear dependence on the parameter $(WV_i)^{1/2}$. The source of the scatter probably lies in the uncertainty of the calculated maximum rim temperature and the velocity at which this temperature occurs, as well as in variations in the ambient air temperature. The straight line fit to the drag braking results does not intercept the origin as one would expect. The cluster of five open circles at around $\eta^* = 20\%$, which is based on the experimental results of Stone and Carpenter (1994), may hold the key to an explanation.

In the experiments of Stone and Carpenter (1994), which incorporated rail heat transfer, it is quite possible that the measured tread temperature is lower than the *true effective* tread temperature. We will presently explain how this is possible by referring again to Figure 3-1. As the wheel rotates and interacts with the brake shoe, a tread *material* element is heated. At point A, this material element has just broken contact with the brake shoe and moves toward the rail contact point B. Point B' represents a position just prior to contact, while B" is the position where contact has just been broken. As was illustrated in the model development (Section 2), the wheel-rail interface (tread) temperature drops to the mean value of the hot wheel and cold rail upon contact. So, the difference in temperature of the material element is large when at locations B' and B". As the element moves toward point C, the tread temperature continuously recovers toward a high value before being heated again by the brake shoe interaction. The location of the sliding contact thermocouple is crucial to the accurate measurement of the effective rim temperature. These details have not been supplied (Stone and Carpenter 1994) but the results shown in Figure 3-3 might suggest that the temperature reported is lower than the effective rim temperature, resulting in an underestimate of η^*. In essence, measuring the rim temperature anywhere between points B" and C may give a tread temperature that is too low for accurately computing the rail heat transfer. A temperature measurement at B' would be more useful for that purpose. However, we used the reported temperatures in our model to estimate η^*. If the actual tread temperature that drives rail heat transfer is higher, then our computation of η^* should be larger, which results in a better linear fit in Figure 3-3.

It is seen that the drag braking data lie on a different line than those for stop braking. The failure to universally correlate the drag and stop braking data lies in the fact that stop braking is a transient process, while drag braking approaches being a steady-state process. The rim temperature, which is not shown, controls the rail heat transfer. In either drag or stop braking, the rail heat transfer should go linearly with the rim temperature, which should go linearly with the heat transfer rate to the rim when the radiation effects are small. However, in drag braking, much lower brake power acts for much longer time periods. This will produce rim temperatures comparable to stop braking, even though the brake power can be an order of magnitude lower. Thus, the value of η^* is much larger in drag braking.

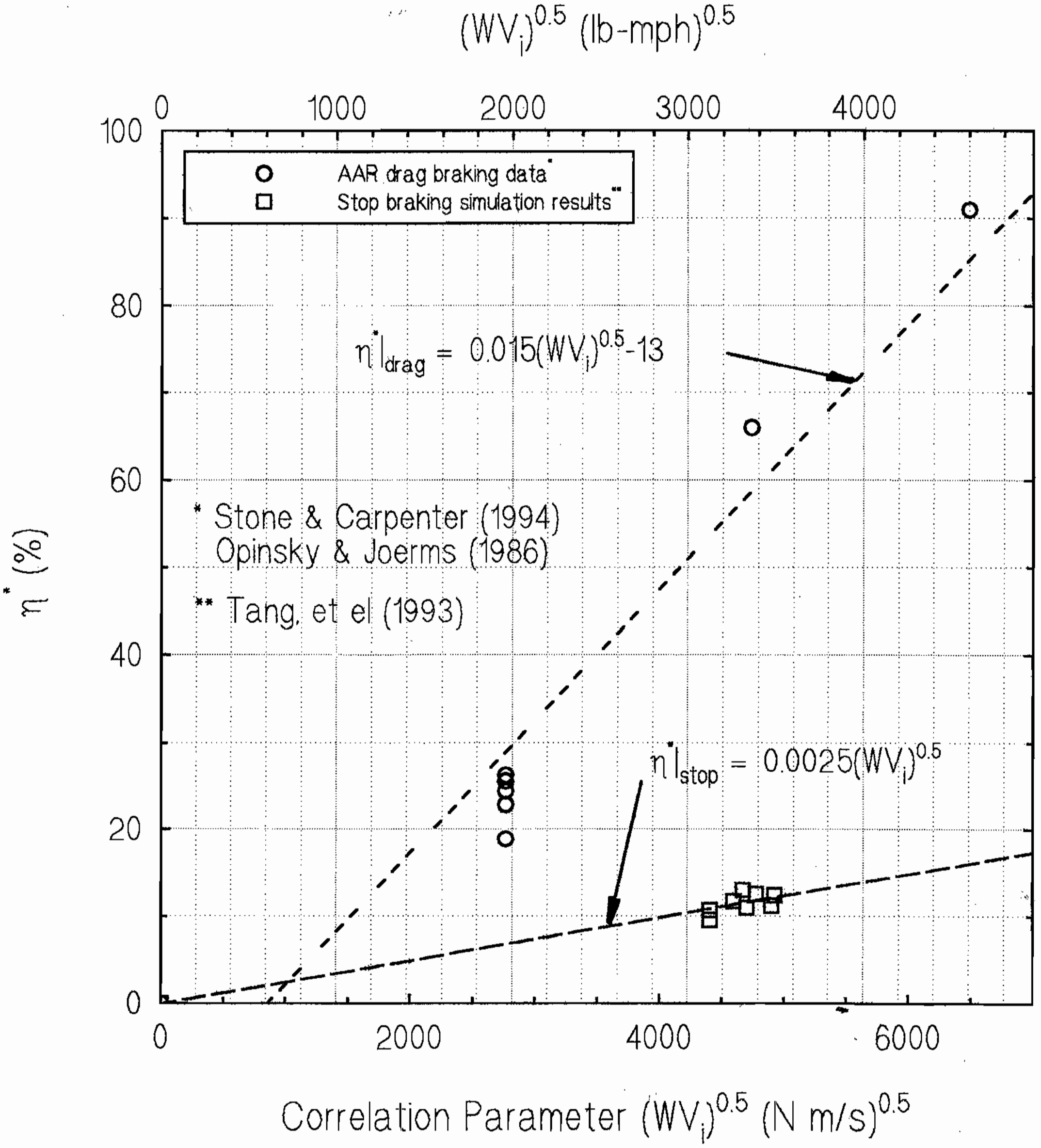

Figure 3-3. **Rail Chill Effectiveness vs. Correlation Parameter for Stop Braking and Drag Braking**

4. DISCUSSIONS AND CONCLUSIONS

4.1 DISCUSSIONS

The results of a simple heat transfer model indicate that the rail chill effectiveness is fairly small under optimum (maximum heat transfer) conditions for stop braking, while rather large for drag braking. The assumptions to simplify the analysis and maximize rail heat transfer were employed, in part, because it was believed the rail chill would in fact be small, providing some justification for not performing a more detailed analysis.

For stop braking, the largest rail chill effectiveness factor η^* was 16%. The estimate, assuming some contact resistance at the interface, drops to less than 10%. The single wheel analysis performed here will not account for rail heat-up when a long series of railcar wheels transfers heat to the rail. Clearly, the effect of rail heat-up in an actual train braking process will reduce the rail effectiveness substantially. Therefore, it is not expected that the rail chill effect will be significant under the typical stop braking conditions.

For drag braking, the picture is different since the rail chill effectiveness factors are large. The largest fractional rail heat transfer rate approaches 100% when contact resistance is neglected. The incorporation of contact resistance reduces the estimates of rail chill effectiveness to about half its value; even then, the rail chill seems to be quite important. More precise estimation of this effect for drag braking would require a more complex heat transfer model. However, the maximum rim temperatures experienced during drag braking are far less damaging than in stop braking, so construction of a more detailed model may not be justified. Further work in this area should focus on the rail heat-up from a multiple wheel analysis.

The computed rail chill effectiveness depends largely on the definition one employs for this parameter. For stop braking, two definitions were employed. First, the ratio of rail heat transfer rate to the rate at which generated heat is transferred to the wheel rim was calculated when the rim temperature was at its maximum (η^*). This approach allows an indirect comparison of rail chill with the other heat loss terms (radiation and convection) since, roughly speaking, the generation and loss terms will balance when the rim temperature reaches its maximum. Thus, the rail chill effectiveness factor we present gives the portion of heat loss credited to rail chill.

Second, the ratio of total rail heat transfer to the total wheel heat transfer evaluated up until the wheel temperature is at its maximum ($\bar{\eta}$) was formulated (employing some modeling assumptions as given in Appendix C). When evaluated with this definition, the rail chill effectiveness is consistently smaller; in fact, about 62% smaller than the value computed with the instantaneous (η^*) value for stop braking. Since $\bar{\eta}$ effectively assesses net heat flow, it may be more useful as a predictor of the maximum wheel rim temperature.

4.2 CONCLUSIONS

The following conclusions have been drawn from the model results regarding the rail chill effect:

1. The magnitude of the rail chill effectiveness depends, to a large degree, on the definition employed. The effectiveness computed based upon instantaneous values of rail heat transfer and heat generation rates will, in general, be larger — by a factor of more than 2 — than that calculated from the integrated (total heat flow) quantities.

2. Based on assumptions that would maximize the rail heat transfer rate, it was found that the rail chill effectiveness factor is no more than 16% for stop braking. Real effects — such as the existence of interface contact resistance, and rail heat-up due to multiple hot wheels rolling past a point on the rail — may reduce the effectiveness to less than 5%.

3. Based on assumptions to maximize the rail heat transfer, it was found that the rail chill effectiveness factor can be as high as 91% for drag braking. However, real effects — such as the existence of interface contact resistance, and rail heat-up for multiple wheels — will reduce this substantially. Because the wheel rim temperatures in drag braking are much lower than in stop braking, further refinement of the rail chill model in this case may not be justified.

4. Based on some first order scaling arguments, the rail chill effectiveness depends linearly on the square root of the railcar's initial momentum.

5. The rail chill heat transfer effectiveness, calculated with the heat transfer model described in this report, agrees closely with the value reported by the Association of American Railroads (AAR).

APPENDIX A

Determination of Wheel-Rail Contact Area, A_c

The following are highlights of a presentation of the theory of H. Hertz, in Timoshenko and Goodier (1951), for computing the area of contact between two cylinders forced together with load, *P*, as illustrated below.

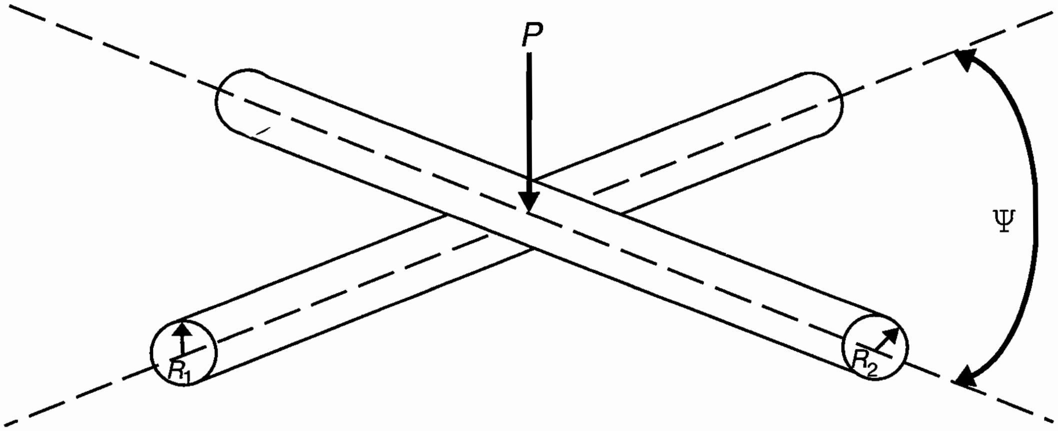

Figure A-1. Area of Contact between Two Cylinders

The region of contact is bounded by an ellipse of major and minor axes 2a and 2b, respectively, as shown below.

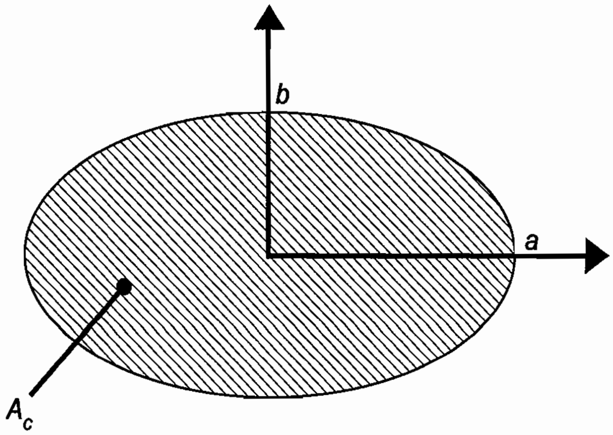

Figure A-2. Region of Contact

The major axis will be parallel to the axis of the smaller radius cylinder. The lengths a and b are found from

$$a = m \sqrt[3]{\frac{3\pi}{4} \frac{P(k_1 + k_2)}{A + B}} \tag{A-1}$$

$$b = n \sqrt[3]{\frac{3\pi}{4} \frac{P(k_1 + k_2)}{A + B}} \tag{A-2}$$

where P is the force of contact. The various parameters in the above equation are defined as follows:

where

$$k_i = \frac{1 - \nu_i^2}{\pi E_i} \qquad \begin{aligned} i &= 1 \ \mathit{for\ cylinder}\ 1 \\ &= 2 \ \mathit{for\ cylinder}\ 2 \end{aligned} \tag{A-3}$$

ν = *Poisson Ratio (assumed same for both cylinders)*
E = *Modulus of Elasticity (assumed same for both cylinders)*

A and B are related to the geometry of each cylinder by

$$A + B = \tfrac{1}{2}\left(\frac{1}{R_1} + \frac{1}{R'_1} + \frac{1}{R_2} + \frac{1}{R'_2} \right) \tag{A-4}$$

$$B - A = \tfrac{1}{2}\left[\left(\frac{1}{R_1} - \frac{1}{R'_1} \right)^2 + \left(\frac{1}{R_2} - \frac{1}{R'_2} \right)^2 + 2\left(\frac{1}{R_1} - \frac{1}{R'_1} \right)\left(\frac{1}{R_2} - \frac{1}{R'_2} \right) \cos 2\Psi \right]^{1/2} \tag{A-5}$$

R_i, R'_i = Principal radii of curvature (in orthogonal directions) for each member at the contact point ($i = 1, 2$)
Ψ = Angle between cylinder axes ($0 < \Psi \leq 90°$)

In this example, $R'_i = \infty$ *and* $\Psi = 90°$.

The above reduces to

$$A = \frac{1}{2R_1}$$
$$B = \frac{1}{2R_2} \tag{A-6}$$

The values of m and n depend on $Arc\,Cos\left(\frac{B-A}{A+B}\right)$ and are tabulated.[1]

Upon solving for a and b, the elliptical area is found from

$$A_c = \pi a b \tag{A-7}$$

---

1. Whittemore H. L. and S. N. Petrenko. 1921. U.S. Bureau of Standards, Technical Paper 201 (or see Ref. 1: 379)

APPENDIX B
Parametric Dependence of Rail Chill

In this appendix, we derive the relationship between the rail chill effectiveness factor and other independent parameters using scaling/dimensional analysis. The rail chill effectiveness factor can be written as a function of the railcar kinematic and other parameters as

$$\dot{Q}_{rail} = f\left(W, \dot{Q}_{gen}, V_i\right) \tag{B-1}$$

The rail heat transfer is given by

$$\dot{Q}_{rail} = \overline{\dot{q}''} A_c = h\, A_c \Delta T \tag{B-2}$$

where

$$\Delta T = T_{int} - T_{rail} \tag{B-3}$$

This temperature difference will scale, to first order, with the wheel heat transfer rate:

$$\dot{Q}_{wheel} \sim \Delta T \sim \dot{Q}_{rail} \tag{B-4}$$

Therefore, we can express the rail chill effectiveness factor as

$$\eta^* = \frac{\dot{Q}_{rail}}{\dot{Q}_{wheel}} \sim h\, A_c = f(W, V_i) \tag{B-5}$$

From Equation 2-8, the heat transfer coefficient is given by

$$h = \frac{k}{\sqrt{\pi \alpha t_c}} \tag{B-6}$$

The contact time, t_c, has been shown from kinematics to be

$$t_c = \frac{\ell}{V} \tag{B-7}$$

where, in this case, V is the car velocity when ΔT is a maximum. We will assume this occurs when $V = V_i / 2$ at time, $t = V_i / 2\, a_d$.

So,

$$V \sim V_i \tag{B-8}$$

The length scale of the elliptical contact area is proportional to the major axis length, $2a$

$$\ell \sim a \sim W^{1/3} \tag{B-9}$$

when the structural properties are fixed. Similarly, the contact area, A_c, has been shown to scale like

$$A_c \sim W^{2/3} \tag{B-10}$$

Combining the results from relations B-5 through B-10 gives the following scaling relationship:

$$\eta^* \sim \frac{\dot{Q}_{rail}}{\dot{Q}_{gen}} \sim \sqrt{W\, V_i} \tag{B-11}$$

So the rail chill effectiveness factor will, to first order, scale with the square root of the initial momentum.

APPENDIX C
Evaluation of Mean Rail Chill Effectiveness Factor

Throughout this report, the rail chill effectiveness has been characterized by the factor,

$$\eta^* \equiv \left. \frac{\dot{Q}_{rail}}{\dot{Q}_{wheel}} \right|_{T = T_{\max}} \tag{C-1}$$

A comparison between this definition and one based on total heat flow is made here. The following simplifying assumptions are made:

- the maximum wheel rim temperature occurs when the railcar velocity is half the initial velocity; and
- the rim temperature rise depends linearly on time until it reaches its maximum temperature.

The plot below illustrates these modeling assumptions.

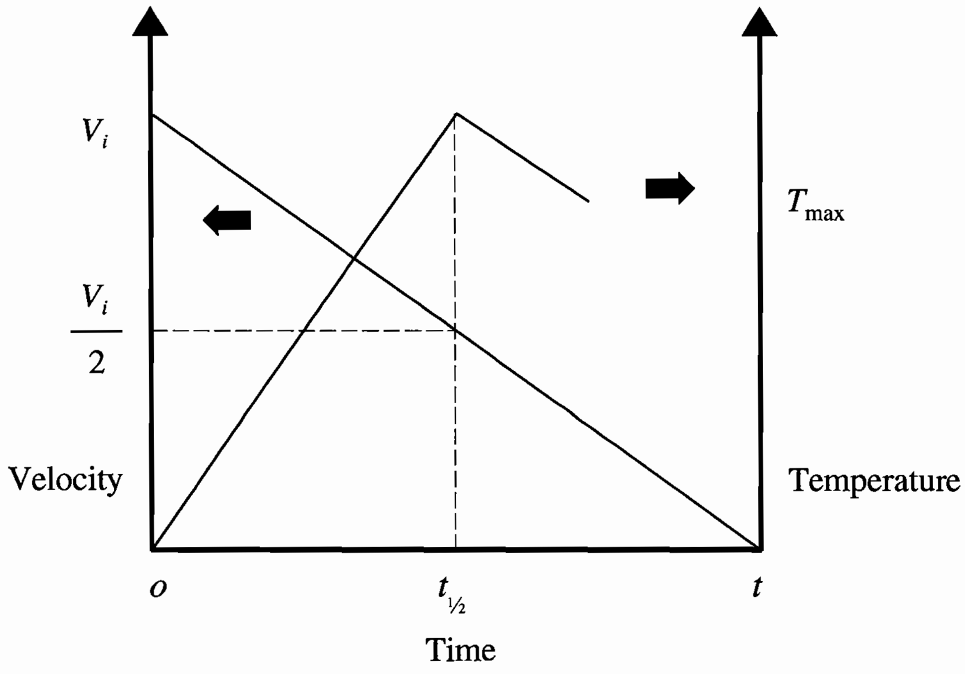

Figure C-1. Modeling Assumptions

We now define a new effectiveness factor, $\bar{\eta}$:

$$\bar{\eta} \equiv \frac{\int_o^{t_{1/2}} \dot{Q}_{rail}\, d\, t}{\int_o^{t_{1/2}} \dot{Q}_{wheel}\, d\, t} \qquad where\ t_{1/2} = \frac{V_i}{2\, a_d} \tag{C-2}$$

To evaluate this quantity, the functional dependence of $\dot{Q}_{rail}$ and $\dot{Q}_{wheel}$ on time, *t*, is required.

Recall,

$$\dot{Q}_{rail} = \dot{q}''_{rail}(t) A_c = \frac{k \Delta T(t)}{\sqrt{\pi \alpha \ell \,/\, V(t)}} A_c \sim \Delta T(t) \sqrt{V(t)} \tag{C-3}$$

and

$$\dot{Q}_{wheel} = m a_d V(t) \sim V(t) \tag{C-4}$$

The value of η^* will depend on the instantaneous values of $\dot{Q}_{rail}$ and $\dot{Q}_{wheel}$ at $t = t_{1/2}$

$$\eta^* = \frac{\dot{Q}_{rail}}{\dot{Q}_{wheel}} \sim \frac{\Delta T_{\max} \sqrt{V_i \,/\, 2}}{V_i \,/\, 2} \tag{C-5}$$

We now define the following dimensionless quantities:

$$\tau \equiv \frac{t}{V_i / a_d}$$

$$v(\tau) = \frac{v(t)}{V_i} = 1 - \tau \tag{C-6}$$

$$\theta(\tau) = \frac{\Delta T(t)}{\Delta T_{\max}} = 2\tau$$

Then,

$$\frac{\bar{\eta}}{\eta^*} = \frac{\int_o^{1/2} \theta(t)\sqrt{2v(t)}\,d\tau}{\int_o^{1/2} v(t)d\tau} = \frac{\int_o^{1/2} 2\tau\sqrt{2(1-\tau)}\,d\tau}{\int_o^{1/2} 2(1-\tau)d\tau} \tag{C-7}$$

Evaluating:

$$\frac{\bar{\eta}}{\eta^*} = \frac{0.14}{0.375} = 0.38 \tag{C-8}$$

Thus, the rail chill effectiveness factor, as defined using the integrated heat transfer, is less than half of the instantaneous value computed at the time when the wheel rim temperature is maximum.

APPENDIX D
Longitudinal Rail Conduction Effects

In the models discussed in Section 2.2 and the results therefrom, we have tacitly ignored the effects of longitudinal (i.e., along the rail) heat conduction effects. The longitudinal conduction has the effect of heating up the rail section ahead of the wheel. The result of this is a reduction in the heat transfer rate to the rail, thereby reducing the rail chill effectiveness so that when the wheel gets there it “feels” a warmer rail. We analyze below the magnitude of reduction of rail chill effectiveness due to longitudinal conduction.

Consider the physical situation indicated in Figure D-1. At an instant of time, $t = 0$, a hot wheel at temperature T_w is brought in contact with a cold rail at temperature $T_{R,\infty}$ and set rolling at a linear velocity, V. Let this initial section be labeled as AA in Figure D-1. Let the position of the wheel, after some short time, be labeled BB.

Figure D-1 also shows the possible variation of the temperature in the rail longitudinally (at, roughly, the top of the rail). The section of rail at BB heats up. It is desired to know (approximately) the new rail surface temperature, T_R, at section BB when the wheel actually arrives at BB. This new rail temperature can be used to determine wheel-to-rail heat flux at BB and, hence, calculate the new rail chill effectiveness.

Using one-dimensional (in x direction) heat transfer, we can show (to a first order accuracy) that the new rail temperature at BB is

$$\frac{T_R - T_{R,\infty}}{T_{int} - T_{R,\infty}} = erfc \, \frac{x}{2\sqrt{\alpha t}} \tag{D-1}$$

where

T_{int} = Wheel-rail interface temperature
x = Distance between sections AA and BB
t = Any time instant since the wheel was at section AA
α = Thermal diffusivity of rail material

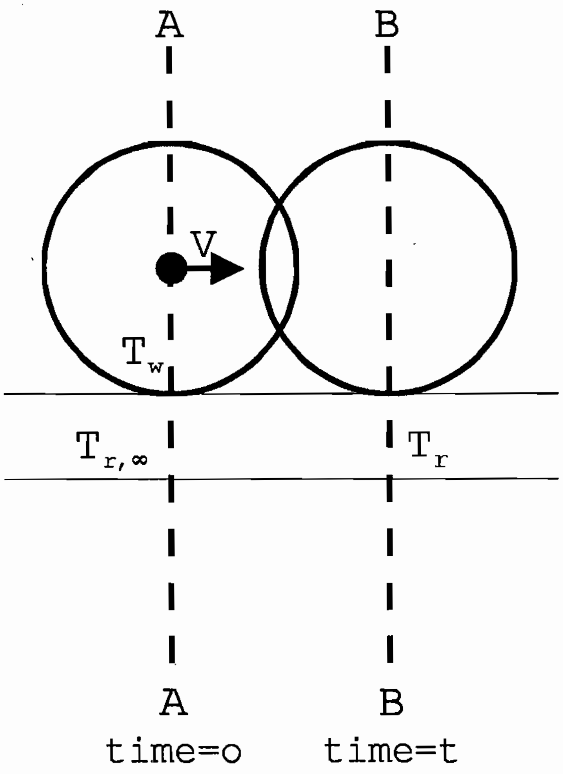
A
B
V
T_w
$T_{r,\infty}$
T_r
A
B
time=o
time=t

Physical Situation

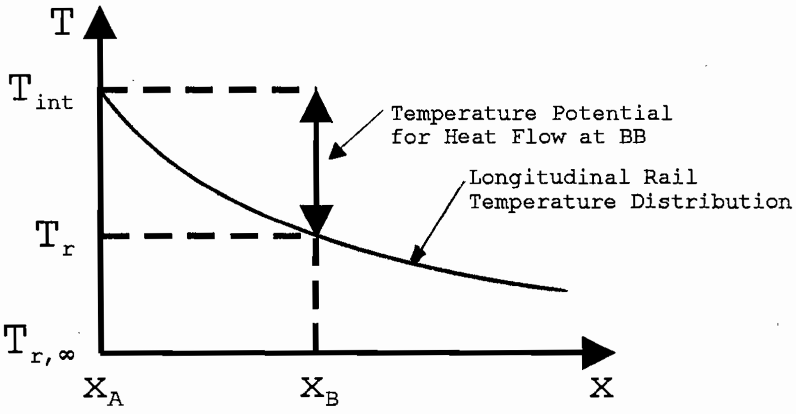
T
T_{int}
Temperature Potential for Heat Flow at BB
Longitudinal Rail Temperature Distribution
T_r
$T_{r,\infty}$
X_A
X_B
X

Longitudinal Temperature Gradient

Figure D-1. Schematic Diagram for Illustrating the Longitudinal Heat Conduction in the Rail

We now define

$$t = \frac{2a}{V} = \textit{time taken for the wheel to move a distance equal to the major axis length of the contact area}$$

$$x = 2a \qquad \text{(D-2)}$$

$$Pe = \frac{V\,a}{\alpha} = \textit{Peclet number}$$

Hence,

$$\frac{T_{int} - T_R}{T_{int} - T_{R,\infty}} = erf\sqrt{\frac{Pe}{2}} \qquad \text{(D-3)}$$

It can be shown (from the definition of heat input rate into the rail – see Equation 2-3 and Equation 2-13) that

$$[\eta]_{k_x} \simeq [\eta]_{k_x=0}\, erf\sqrt{\frac{Pe}{2}} \qquad \text{(D-4)}$$

where

$[\eta]_{k_x}$ = Rail chill effectiveness when the longitudinal conduction in the rail is considered

$[\eta]_{k_x=0}$ = Rail chill effectiveness when rail longitudinal conduction is neglected

For the cases illustrated in Table 2-1, the value of *Pe* is of the order of magnitude 25,000. For this value, the error function on the right-hand side of Equation D-4 is essentially 1. That is, the conduction effects, longitudinally, are negligible.

APPENDIX E

Relation between Wheel Temperature and Brake Power Input

In this appendix we develop a simple model of the heat transfer interaction between the brake shoe and wheel to help explain some unexpected results in Figure 3-2 of Section 3, where the wheel temperature vs. brake power data of Stone and Carpenter (1994) is plotted. The data follow a straight line, but are clearly displaced from intersecting the origin (ambient temperature at zero power). This model is intended to illustrate, at least qualitatively, why simple linear behavior is not seen. Figure E-1 illustrates the brake shoe-wheel interface region. Though the heat transferred to the wheel is distributed around the circumference, at any instant, the heat transfer area for the wheel is equal to that of the shoe, so the following analysis is expressed solely in terms of heat fluxes. In the following model, the subscripts *w*, *s*, and *c* refer to the wheel, brake shoe, and contact region, respectively. We assume that braking induces a volumetric heat generation, q'''_{gen}, within a finite thickness in the interface region, δ.

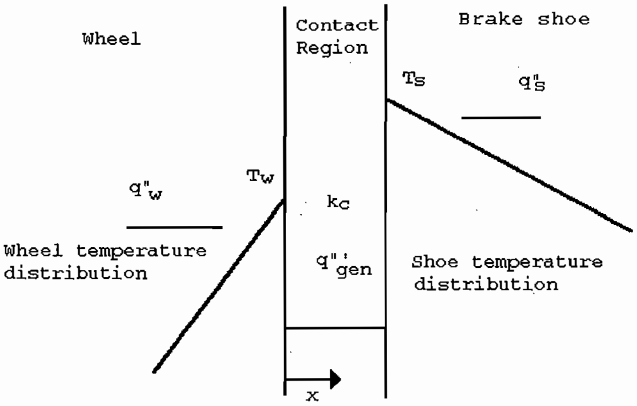

Figure E-1. Brake Shoe-Wheel Interface Region

In this region, the steady heat conduction equation is

$$q'''_{gen} = -k_c \frac{d^2T}{dx^2} \qquad \text{(E-1a)}$$

subject to the following boundary conditions:

$$k_c \frac{dT}{dx}\Big|_{x=0} = q''_w \tag{E-1b}$$

$$T(0) = T_w \tag{E-1c}$$

The solution is then given by

$$T(x) = -\frac{q'''_{gen}\, x^2}{2k_c} + \frac{q''_w\, x}{k_c} + T_w \tag{E-2}$$

The shoe surface temperature is found from

$$T_s = T(\delta) = -\frac{q'''_{gen}\, \delta^2}{2k_c} + \frac{q''_w \delta}{k_c} + T_w \tag{E-3}$$

This equation may be simplified by defining the contact heat transfer coefficient, $h_c = k_c/\delta$, and relating the volumetric heat generation rate to the generated heat flux:

$$q''_{gen} = q'''_{gen}\, \delta \tag{E-4}$$

Equation E-3 is then written

$$T_s - T_w = -\frac{q''_{gen}}{2h_c} + \frac{q''_w}{h_c} \tag{E-5}$$

To eliminate the shoe surface temperature from Equation E-5, we relate the shoe heat flux to the shoe temperature assuming an ambient temperature of 0°C:

$$q''_s = h_s T_s \tag{E-6}$$

Also, the shoe heat flux can be eliminated using the energy balance,

$$q''_s = q''_{gen} - q''_w \tag{E-7}$$

Combining the last three equations, we can express the wheel temperature in terms of q''_{gen} and h_c:

$$T_w = q''_{gen}\left(\frac{1}{h_s} + \frac{1}{2h_c}\right) - q''_w\left(\frac{1}{h_s} + \frac{1}{h_c}\right) \tag{E-8}$$

We now express q''_w as some fraction, f, of the total generated heat flux, q''_{gen}:

$$q''_w = f\, q''_{gen} \tag{E-9}$$

Equation E-8 then becomes

$$T_w = q''_{gen}\left[\left(\frac{1-f}{h_s}\right) + \left(\frac{1/2\ -f}{h_c}\right)\right] \tag{E-10}$$

The brake shoe-wheel thermal contact conductance, h_c, will depend on the magnitude of the normal force between the shoe and wheel, P. For the purpose of illustration, we assume that $h_c \sim P$. Since $q''_{gen} \sim P$ for fixed speed, it follows that $h_c \sim q''_{gen}$. Equation E-10 takes the form

$$T_w = A\, q''_{gen} - B \tag{E-11}$$

where A and B are constants. In practice, the fraction of heat flux that is transferred to the wheel is more than half but less than unity; so $0.5 < f < 1.0$. Therefore, A and B are both positive. The straight line (offset from the origin) represented by Equation E-11 resembles the data of Figure 3-2, which is the measured steady-state wheel temperature at various brake power levels (Stone and Carpenter 1994). Clearly, this result will not apply for very low power levels since the wheel temperature would then be negative. In reality, the relation between h_c and q''_{gen} is more complex than we have assumed. However, this model was used to illustrate how variable contact resistance between the brake shoe and wheel results in a non-linear relationship between T_{wheel} and $\dot{Q}_{gen}$.

NOMENCLATURE

A	area	cm^2
a_d	deceleration	m/s^2 *or* mph/s
a	ellipse half axis	m
b	ellipse half axis	m
c	specific heat	J/kg K
D	diameter	m
h	heat transfer coefficient	W/m^2 K
k	thermal conductivity	W/m K
ℓ	average contact length	m
m	railcar mass	kg
P	single wheel load	N
$\wp$	power	W
Pe	Peclet number	-
$\dot{q}''$	heat flux rate	W/m^2
Q	heat transfer	J
$\dot{Q}$	heat transfer rate	W
R	thermal resistance	°C/W
R	radius	m
t	time	s
t_c	contact time	s
T	temperature	°C
V	velocity	m/s *or* mph
W	railcar weight	N *or* lbs.

NOMENCLATURE (continued)

Greek

α	thermal diffusivity	m^2/s
δ	thermal penetration depth or thickness	m
η	effectiveness factor	-
ρ	density	kg/m^3
σ_y	yield strength	Pa
τ	dimensionless time	-

Subscripts

a	ambient
bl	boundary layer
c	contact
conv	convection
gen	generated
i	initial
int	interface
max	referring to a maximum condition

REFERENCES

1. Fenech, H. and W. M. Rohsenow. 1963. Prediction of Thermal Conductance of Metallic Surfaces in Contact. *J. Heat Transfer, Trans. ASME* 85, Feb: 15–24.

2. Opinsky, A. J. and M. W. Joerms. 1986. *Finite Element Stress Analysis of Three Edgewater 32 Inch Wheel Designs*. Chicago: Association of American Railroads, Chicago Technical Center. Report no. LT-638.

3. Rohsenow, W. M. and J. P. Hartnett, eds. 1973. *Handbook of Heat Transfer*. McGraw-Hill: 3.14–18.

4. Stone, D. H. and G. F. Carpenter. 1994. Wheel Thermal Damage Limits. *Proc. ASME/IEEE Joint Railroad Conf.*, Chicago, IL.

5. Stone, D. H. and G. J. Moyar. 1989. Wheel Shelling and Spalling – An Interpretive Review. *Proc. ASME Winter Annual Meeting.*

6. Tang, Y. H., J. E. Gordon, A. B. Perlman, and O. Orringer. 1993. *Finite Element Models, Validation, and Results for Wheel Temperature and Elastic Thermal Stress Distributions.* Volpe National Transportation Systems Center. Report no. DOT/FRA/ORD-93/17.

7. Timoshenko, S. and J. N. Goodier. 1951. *Theory of Elasticity* (Second edition). McGraw-Hill.

REPORTS IN THIS SERIES

1. Orringer, O., D. E. Gray, and R. J. McCown. 1993. *Evaluation of Immediate Actions Taken to Deal with Cracking Problems in Wheels of Rail Commuter Cars.* Volpe National Transportation Systems Center. Report no. DOT/FRA/ORD-93/15.

2. Tang, Y. H., J. E. Gordon, A. B. Perlman, and O. Orringer. 1993. *Finite Element Models, Validation, and Results for Wheel Temperature and Elastic Thermal Stress Distributions.* Volpe National Transportation Systems Center. Report no. DOT/FRA/ORD-93/17.

3. Tang, Y. H., J. E. Gordon, O. Orringer, and A. B. Perlman. 1993. *Stress Reconstruction Analysis of Wheel Saw Cut Tests and Evaluation of Reconstruction Procedure.* Volpe National Transportation Systems Center. Report no. DOT/FRA/ORD-93/18.

4. Stuart, C. 1993. *Thermal Measurements of Commuter Rail Wheels Under Revenue Service Conditions.* ENSCO, Inc. Report no. DOT/FRA/ORD-93/19.

5. Pelloux, R. M., and D. C. Grundy. 1994. *Thermomechanical Testing and Microstructural Development of Class L Steel Wheel Alloy.* Department of Materials Science and Engineering, MIT. Report no. DOT/FRA/ORD-94/01.

6. Gordon, J. E. and O. Orringer. 1996. *Investigation of the Effects of Braking System Configurations on Thermal Input to Commuter Car Wheels.* Volpe National Transportation Systems Center. Report no. DOT/FRA/ORD-96/01.

7. Bobrov, E. S. and M. Holowinski. 1996. *Estimation of Actual Residual Stresses Due to Braking and Contact Loading of Rail Vehicle Wheels.* Francis Bitter National Magnet Laboratory, MIT. Report no. DOT/FRA/ORD-96/02.